Nature of Oxygen Activation in Glucose Oxidase from *Aspergillus niger*: The Importance of Electrostatic Stabilization in Superoxide Formation†

Qiaojuan Su and Judith P. Klinman*

Department of Chemistry, University of California, Berkeley, California 94720

Received January 7, 1999; Revised Manuscript Received May 3, 1999

ABSTRACT: Glucose oxidase catalyzes the oxidation of glucose by molecular dioxygen, forming gluconolactone and hydrogen peroxide. A series of probes have been applied to investigate the activation of dioxygen in the oxidative half-reaction, including pH dependence, viscosity effects, ^{18}O isotope effects, and solvent isotope effects on the kinetic parameter $V_{max}/K_m(O_2)$. The pH profile of $V_{max}/K_m(O_2)$ exhibits a pK_a of 7.9 ± 0.1, with the protonated enzyme form more reactive by 2 orders of magnitude. The effect of viscosogen on $V_{max}/K_m(O_2)$ reveals the surprising fact that the faster reaction at low pH (1.6×10^6 M^{-1} s^{-1}) is actually less diffusion-controlled than the slow reaction at high pH (1.4×10^4 M^{-1} s^{-1}); dioxygen reduction is almost fully diffusion-controlled at pH 9.8, while the extent of diffusion control decreases to 88% at pH 9.0 and 32% at pH 5.0, suggesting a transition of the first irreversible step from dioxygen binding at high pH to a later step at low pH. The puzzle is resolved by ^{18}O isotope effects. $^{18}(V_{max}/K_m)$ has been determined to be 1.028 ± 0.002 at pH 5.0 and 1.027 ± 0.001 at pH 9.0, indicating that a significant O−O bond order decrease accompanies the steps from dioxygen binding up to the first irreversible step at either pH. The results at high pH lead to an unequivocal mechanism; the rate-limiting step in $V_{max}/K_m(O_2)$ for the deprotonated enzyme is the first electron transfer from the reduced flavin to dioxygen, and this step accompanies binding of molecular dioxygen to the active site. In combination with the published structural data, a model is presented in which a protonated active site histidine at low pH accelerates the second-order rate constant for one electron transfer to dioxygen through electrostatic stabilization of the superoxide anion intermediate. Consistent with the proposed mechanisms for both high and low pH, solvent isotope effects indicate that proton transfer steps occur after the rate-limiting step(s). Kinetic simulations show that the model that is presented, although apparently in conflict with previous models for glucose oxidase, is in good agreement with previously published kinetic data for glucose oxidase. A role for electrostatic stabilization of the superoxide anion intermediate, as a general catalytic strategy in dioxygen-utilizing enzymes, is discussed.

Glucose oxidase (GO,[1] β-D-glucose:oxygen 1-oxidoreductase, EC 1.1.3.4), a homodimer flavoprotein consisting of 1 mol of FAD per subunit, catalyzes the oxidation of β-D-glucose to δ-gluconolactone, which subsequently hydrolyzes spontaneously to gluconic acid, concomitant with the reduction of dioxygen to hydrogen peroxide. GO has been isolated from red algae, citrus fruits, insects, bacteria, and molds (*1*). GO from *Aspergillus niger* has been cloned and expressed in yeast (*2*, *3*). The molecular mass varies from 130 to 325 kDa depending on the degree of glycosylation. The catalytic activity of the recombinant and the wild-type enzymes is similar, and changes in glycosylation do not cause significant changes in the structure or turnover number (*4*−*6*).

The GO reaction proceeds through a ping-pong mechanism (*7*) shown in eqs 1 and 2:

$$E_{ox} + \text{glucose} \rightarrow E_{red} + \text{gluconolactone} \quad (1)$$

$$E_{red} + O_2 \rightarrow E_{ox} + H_2O_2 \quad (2)$$

where E_{ox} is the resting enzyme with FAD in the oxidized form and E_{red} is the enzyme with FAD in the reduced form resulting from the reductive half-reaction. The substrates of GO include D-glucose, D-galactose, D-xylose, D-mannose, and 2-deoxy-D-glucose, among which D-glucose is by far the most effective substrate and 2-deoxy-D-glucose is the slowest substrate. The crystal structure of GO from *A. niger* was determined at 2.3 Å resolution (*8*). Figure 1 illustrates the active site structure of GO, showing the binding of the flavin in relation to protein side chains within the enzyme active site.

Two mechanisms have been proposed for the reductive half-reaction (Scheme 1): (i) hydride transfer from substrate C-1 to flavin N-5 and (ii) nucleophilic addition by the substrate OH group at C-1 to the C-4a position of the flavin, followed by proton abstraction from C-1 of the substrate (*9*−*11*). Despite the fundamental differences between these two mechanisms, both are expected to be assisted by general base catalysis. A close inspection of the active site (Figure 1)

† This research was supported by National Institutes of Health Grant GM 25765.

* To whom correspondence should be addressed. J.P.K. is also in the Department of Molecular and Cell Biology at the University of California, Berkeley.

[1] Abbreviations: GO, glucose oxidase; FAD, flavin adenosine dinucleotide; Fl_{red}, flavin in the reduced form; Fl_{sq}, flavin in the semiquinone form; Fl_{ox}, flavin in the oxidized form; AO, alcohol oxidase; CO, cholesterol oxidase; SHE, standard hydrogen electrode.

10.1021/bi990044o CCC: $18.00
Published on Web 06/10/1999

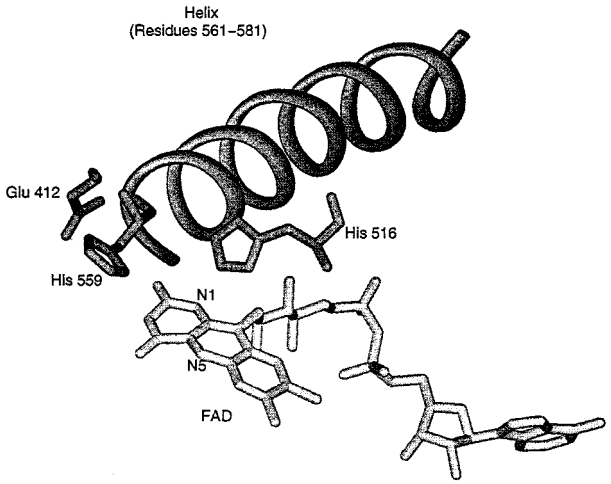

FIGURE 1: Illustration of the active site of the *A. niger* glucose oxidase. Coordinates were taken from Brookhaven Protein Data Bank file name 1GAL. The figure was generated using Insight II 95.0.

Scheme 1: Two Proposed Mechanisms for the Reductive Half-Reaction in Glucose Oxidase

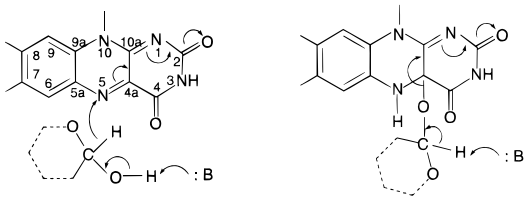

indicates that His 516, positioned on top of the isoalloxazine ring, is a potential proton acceptor: Nϵ of His 516 is 3.80 Å away form N-1 of FAD, 3.78 Å from C-4a of FAD, and 3.43 Å from C-10a of FAD. Another possible candidate for the functional catalytic base is His 559, located to the left side of FAD: Nδ of His 559 is 3.57 Å away from N-3 of FAD.

As a result of the reductive half-reaction, two electrons and two protons have been transferred to enzyme, presumably at the site of the reduced flavin ($2e^-$ and $1H^+$) and the protonated histidine ($1H^+$). In the oxidative half-reaction, the stored electrons and protons are transferred to dioxygen to yield H_2O_2, and the catalytic cycle is complete. Previous studies have applied stopped flow methods (*7*, *11*−*13*) and rapid quench ESR spectroscopy (*13*) to the oxidative half-reaction. In no case has flavin semiquinone been detected as an intermediate, and there has been no evidence for the formation of the $E_{red}{\cdot}O_2$ complex (*7*). The following questions remain unanswered with regard to the oxidative half-reaction. (i) What is the nature of the rate-determining step(s)? (ii) To what extent (if any) are the steps involving proton and electron transfer coupled? (iii) What are the strategies that the enzyme applies to activate the kinetically very sluggish dioxygen molecule? In an attempt to address the question of dioxygen activation in enzyme-catalyzed reactions, a series of experimental protocols have been developed that allow detailed characterization of dioxygen reduction mechanisms (*14*). In this work, ^{18}O isotope effects, viscosity effects, and solvent isotope effects have been determined and are discussed in the context of pH effects. These studies lead to the identification of rate-limiting steps, together with a model in which electrostatic stabilization via an active site $HisH^+$ provides a key role in the formation and stabilization of a superoxide anion intermediate.

EXPERIMENTAL PROCEDURES

Materials

The commercially available wild-type GO was not used because it contains small amounts of catalase, which catalyzes the disproportionation of H_2O_2 and could interfere with accurate determinations of steady-state rates and ^{18}O isotope effects. The lyophilized recombinant enzyme from *A. niger* expressed in *Saccharomyces cerevisiae* (*3*) (molecular mass of 325 ± 50 kDa) was used in this work. To correct for small changes in enzyme activity, a standard enzyme assay was carried out in conjunction with each set of rate measurements. Standard enzyme assays employed 0.5 M 2-deoxy-D-glucose as the substrate in 100 mM sodium acetate buffer at pH 5.0 and 25 °C, and were monitored by the decrease of oxygen concentration. The ratio of the observed rate to 41.7 s^{-1} provided a correction factor that was then applied to all measurements within a given set. All other materials were obtained commercially and were reagent grade.

Methods

Steady-State Kinetics. Initial velocity studies were carried out at 25 °C by following dioxygen consumption on a Yellow-Springs 5300 oxygen monitor. It was reported that the oxidative half-reaction is pH-dependent and ionic strength affects the pK_a (*15*, *16*). As chloride and other halide ions have been demonstrated to be GO inhibitors (*17*), the conventional method of ionic strength adjustment through addition of salts was not applied. Maintaining a constant ionic strength while minimizing any effect from addition of extra anions was achieved by varying the concentrations of the buffers. The following buffers were used: 0.163 M sodium acetate at pH 5.0, 0.0890 M potassium phosphate at pH 6.0, 0.0566 M potassium phosphate at pH 7.0, 0.0162 M sodium pyrophosphate at pH 8.0, 0.0136 M sodium pyrophosphate at pH 9.0, and 0.0107 M sodium pyrophosphate at pH 10.0. The concentration of 2-deoxy-D-glucose was 0.3 M in all assay solutions. The effect of buffer concentration is considered to be insignificant, since similar results were obtained when a different set of buffer concentrations was employed (*35*). In particular, kinetic parameters measured at pH 5.0 with a range of different buffer concentrations (0.163, 0.100, and 0.0094 M) are within experimental error (data not shown). Steady-state parameters were obtained by a nonlinear fit to the Michaelis−Menten equation using the program KaleidaGraph on a Macintosh computer.

Viscosity Effects. Viscosity effect studies were performed at pH 5.0, 9.0, and 9.8. Substrate solutions with various relative viscosities were prepared by adding ethylene glycol as the viscosogen. Buffer contents for solutions at pH 5.0 and 9.0 are described above; solutions at pH 9.8 contained 0.0111 M sodium pyrophosphate. With ethylene glycol concentrations of 0, 16, 28, 36, and 44 wt %, relative viscosities ranging from 1 to 3 were obtained. The viscosities were determined by measuring the time for the solutions to flow through an Ostwald viscometer kept at 25 °C. The relative viscosities were calculated using the same buffered

substrate solution, without ethylene glycol, as the reference. Steady-state parameters for all the solutions were determined as described in Steady-State Kinetics.

Isotope Effects. ^{18}O kinetic isotope effects were measured at 20 °C and pH 5.0 and 9.0 in the presence of ca. 1 mM O_2 and 50 mM 2-deoxy-D-glucose. The reaction was coupled with horseradish peroxidase using guaiacol as the substrate to convert H_2O_2 to H_2O. The measurements were obtained as previously described (*14*). Solvent isotope effects were investigated through measurement of $V_{max}/K_m(O_2)$ in a series of D_2O solutions with various pD values. The enzyme solution was lyophilized and dissolved in D_2O three times to remove H_2O. Substrate solutions contained 0.3 M 2-deoxy-glucose and buffering compounds with the same concentrations listed in Steady-State Kinetics. Dry components were dissolved in D_2O, and the pD was adjusted with potassium hydroxide or acetic acid (both dissolved in D_2O). The initial solutions were then lyophilized and redissolved in D_2O three times. The final pD value was measured using a regular pH electrode, adding 0.4 to the original reading (*18*, *36*, *37*). The steady-state kinetics were examined at different pD values, and the pD profile was compared to the pH profile.

Simulation of the Oxidative Half-Reaction. An SGI version of the KINSIM program (*19*) was applied to simulate the stopped flow trace of flavin semiquinone (Fl_{sq}) upon mixing of the reduced GO with dioxygen at pH 5.0. The mechanism that was used was as follows:

$$E-Fl_{red} + O_2 \underset{k_{-1}}{\overset{k_1}{\rightleftharpoons}} E-Fl_{sq}\cdot O_2^{-\bullet} \quad (3)$$

$$E-Fl_{sq}\cdot O_2^{-\bullet} \xrightarrow{k_2} E-Fl_{ox}-OO^- \quad (4)$$

$$E-Fl_{ox}-OO^- \xrightarrow{k_3} E-Fl_{ox}-OOH \quad (5)$$

$$E-Fl_{ox}-OOH \xrightarrow{k_4} E-Fl_{ox} + HOOH \quad (6)$$

where k_1 was fixed at 5.7×10^6 M^{-1} s^{-1}, k_{-1} was varied in a range from 10^7 to 10^2 s^{-1}, and k_2 was adjusted accordingly by keeping the ratio of k_{-1}/k_2 equal to 2; k_3 and k_4 were assigned values so that $k_4 \gg k_3 \gg k_2$.

RESULTS

pH Dependence of $V_{max}/K_m(O_2)$. A series of probes were applied to characterize different aspects of the kinetic parameter $V_{max}/K_m(O_2)$, which reflects all steps from the binding of dioxygen up to and including the first irreversible step in the oxidative half-reaction. Initial experiments focused on the pH dependence. The oxidative half-reaction has been shown to be dependent on pH when glucose is used as the substrate (*9*, *11*, *15*). In this work, $V_{max}/K_m(O_2)$ is measured at different pH values with 2-deoxy-D-glucose as the substrate, with the results shown in Figure 2. Consistent with the proposed ping-pong mechanism (*7*), the pH profiles of the oxidative half-reaction with two different substrates are very similar, suggesting that the oxidation product of the first substrate has been released from the active site of the enzyme before dioxygen binds so that the oxidative half-reaction proceeds without influence from the first substrate. The pH profile shows a dependence of the oxidative half-reaction on the protonation of a single group. However, there are two possible models for the interpretation of the observed pH profile: (i) a one-state model (*11*, *15*), where only the protonated form of enzyme is active, indicating that $V_{max}/K_m(O_2)$ should diminish at high pH and (ii) a two-state model (*9*), where both protonated and deprotonated forms of the enzyme are active but catalyze the oxidative half-reaction with different efficiencies. Although the observed data fit the two-state model better (Figure 2), this may result from the larger number of parameters used in the two-state model. Discrimination between these two models would require measurements of $V_{max}/K_m(O_2)$ at even higher pH values, where accurate data acquisition is impaired by several factors, including decreased enzyme stability and the use of a possibly inhibitory buffer system [inferred from the inhibition by putrescine (*16*) and our observation of an inhibitory effect from Tris buffer (data not shown)]. Effective mechanistic probes could resolve this ambiguity indirectly. The one-state model predicts that a single mechanism works throughout the pH range; in contrast, the two-state model argues that there exist two different mechanisms leading to different catalytic efficiencies. As will be shown below, using viscosity effects, different extents of diffusion control were found at different pH values, suggesting that more than one mechanism exists for the oxidative half-reaction. Therefore, both protonated and deprotonated enzyme forms are concluded to be active. The fitting using the two-state model gives a pK_a of 7.9 ± 0.1, in agreement with previous results. Voet et al. (*15*) observed that this pK_a varies from 8.2 to 7.3 with a range of ionic strength from 0.025 to 0.225 M, and calculated that the intrinsic pK_a is 6.7. The intrinsic pK_a is consistent with assignment to the active site histidine. However, the N-1 position of reduced flavin has also been shown to have a pK_a of 6.7 in solution (*20*) such that the observed pH profile could reflect ionization of the reduced flavin as opposed to the active site histidine. Arguments against this possibility follow. First, the redox potential of the free flavin has been found to decrease with increasing pH (*21*); i.e., the flavin becomes a better reductant as it becomes deprotonated. If the ionization observed for $V_{max}/K_m(O_2)$ were due to the ionization of the flavin, the rate would have been expected to increase (rather than decrease) with increasing pH. Second, NMR studies of the reduced

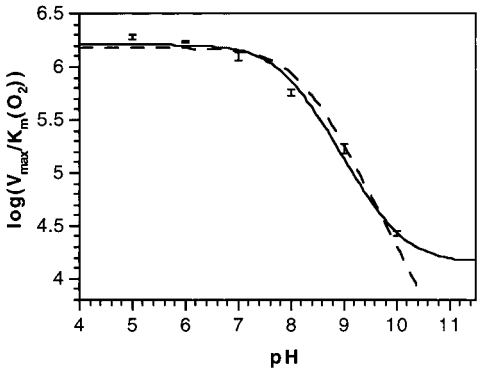

FIGURE 2: pH dependence of $V_{max}/K_m(O_2)$ using 2-deoxy-D-glucose as the substrate. The solid line is a fit of experimental data to a two-state model: $\log[V_{max}/K_m(O_2)] = \log[\text{Min}/(1 + 10^{pK_a - pH}) + \text{Max}/(1 + 10^{pH - pK_a})]$. The dashed line is a fit to a one-state model: $\log[V_{max}/K_m(O_2)] = \log[\text{Max}/(1 + 10^{pH - pK_a})]$ (see the text). The parameters pK_a, Min, and Max are obtained from the fitting.

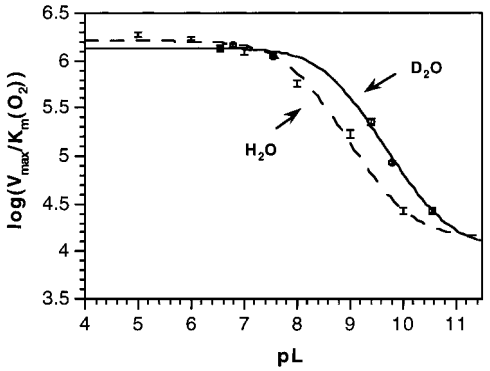

FIGURE 3: Solvent isotope effects on $V_{max}/K_m(O_2)$. Lines are fit to the following equation: $\log[V_{max}/K_m(O_2)] = \log[\mathrm{Min}/(1 + 10^{pK_a - pL}) + \mathrm{Max}/(1 + 10^{pL - pK_a})]$. pL represents pH (in H_2O) or pD (in D_2O). The maximum $V_{max}/K_m(O_2)$ is $(1.6 \pm 0.2) \times 10^6$ M^{-1} s^{-1} in H_2O and $(1.4 \pm 0.1) \times 10^6$ M^{-1} s^{-1} in D_2O; the minimum $V_{max}/K_m(O_2)$ is $(1.4 \pm 0.8) \times 10^4$ M^{-1} s^{-1} in H_2O and $(1.1 \pm 0.4) \times 10^4$ M^{-1} s^{-1} in D_2O.

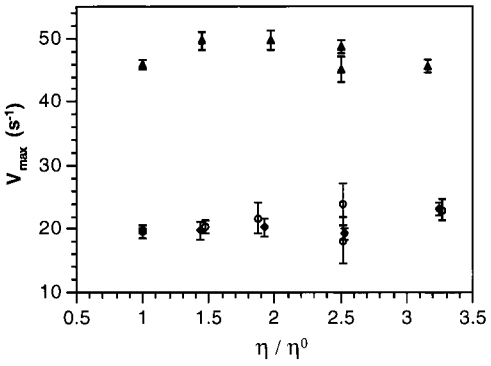

FIGURE 4: Effect of viscosity on V_{max} when ethylene glycol is used as the viscosogen. $\eta/\eta°$ is the relative viscosity (η_{rel}): pH 5.0 (▲), 9.0 (◆), and 9.8 (●).

flavin in *A. niger* GO indicate that the N-1 position of the cofactor is anionic at pH 5.6 (*22*); i.e., the pK_a for the flavin has been significantly perturbed in its enzyme-bound state. From the X-ray structure of the *A. niger* GO (cf. Figure 1), the Nϵ of His 516 is located approximately 3.80 Å from the N-1 position of the cofactor (*8*), close enough to bring about a significant pK_a perturbation. Collectively, the available facts lead to an assignment of the species within the low-pH form of reduced enzyme to the flavin monoanion and protonated histidine. In this manner, the ionization affecting V_{max}/K_m (O_2) is assigned to the active site histidine. The limiting values for V_{max}/K_m (O_2) are $(1.6 \pm 0.2) \times 10^6$ M^{-1} s^{-1} (at low pH) and $(1.4 \pm 0.8) \times 10^4$ M^{-1} s^{-1} (at high pH). The deprotonated form reacts with dioxygen ca. 100-fold slower than the protonated form. Probes are described below with the goal of inferring how different protonation states of an active site group alter the mechanism of the oxidative half-reaction and lead to different reactivities toward dioxygen.

Solvent Isotope Effects. The increase in rate with protonated histidine suggested the possibility of general acid catalysis, such that proton and electron transfer were concomitant processes at low pH. This was addressed by examining V_{max}/K_m (O_2) in D_2O, with the results shown in Figure 3. Although the pH-dependent curve is found to shift in D_2O to a more basic pK_a ($\Delta pK_a = 0.7$), the limiting rate constants at high and low pH are only modestly changed: $(1.4 \pm 0.1) \times 10^6$ (low pD) and $(1.1 \pm 0.4) \times 10^4$ M^{-1} s^{-1} (high pD). Since D_2O has a higher viscosity than H_2O, small decreases in V_{max}/K_m (O_2) could reflect slower diffusion rates. As we show below, the reaction of GO with dioxygen is partially diffusion-controlled at low pH and fully diffusion-controlled at high pH. Thus, the observed effects of D_2O on $V_{max}/K_m(O_2)$ can be fully explained by the degree of rate limitation by diffusion at each pH. It is concluded that proton transfer from a protonated $HisH^+$ to dioxygen does not occur in the rate-determining step of $V_{max}/K_m(O_2)$.

Viscosity Effects. Dioxygen is a small hydrophobic molecule lacking dipolar character. In most biological systems, dioxygen is observed to bind to a redox active metal site, undergoing a charge transfer interaction in the course of its binding. In the absence of a protein-bound metal site with the correct redox character, dioxygen may prebind into a hydrophobic site (*14*) or it may react in a diffusion-limited process to yield the first catalytic intermediate. In previous works on the oxidative half-reaction of GO, no semiquinoid intermediate was detected and there was no evidence for the formation of an enzyme−oxygen complex (*7*, *11*−*13*). The obvious explanation for this observation is that binding of oxygen is the slow and first irreversible step, as shown in eq 7:

$$E_{red} + O_2 \xrightarrow{\text{slow, } k_1} \qquad (7)$$

However, since the solubility of molecular oxygen is very limited (1.2 mM at 25 °C), the reversible formation of the initial $E_{red}{\cdot}O_2$ complex with a K_d value greater than the saturated oxygen concentration cannot be ruled out. This alternative mechanism can be written as eq 8:

$$E_{red} + O_2 \underset{k_{-1}}{\overset{\text{fast, } k_1}{\rightleftharpoons}} E_{red}{\cdot}O_2 \xrightarrow{k_2} \qquad (8)$$

Evidence for rate-limiting substrate association, as described in eq 7, can often be obtained from viscosity effects. Since an increase in viscosity lowers the diffusion rate, which directly slows the encounter rate of two molecules, a decrease in the reaction rate is anticipated (*23*). In contrast, if an $E_{red}{\cdot}O_2$ complex actually forms and decomposes rapidly according to eq 8, both association and dissociation rates of dioxygen relative to the enzyme should be lowered in a similar manner with increasing viscosity, while the rate of some other slow chemical step would be unperturbed. In this instance, varying viscosity would not be expected to have a significant effect on $V_{max}/K_m(O_2)$.

An important control for nonspecific and rate-altering effects of viscosogen is the absence of a measurable decrease in V_{max} values with increasing viscosogen concentrations. Using D-glucose as the substrate, the K_m of O_2 for GO at high pH is greater than the dissolved concentration of 100% dioxygen, such that accurate measurement of V_{max} is impossible at atmospheric pressure. The slower substrate, 2-deoxy-D-glucose, results in a much smaller K_m for O_2 and therefore was chosen as the substrate for this study. As shown in Figure 4, V_{max} is essentially unchanged when ethylene glycol is used as the viscosogen. The unperturbed V_{max} argues against an inhibitory effect of ethylene glycol and, further, that product diffusion from the active site is not a rate-limiting step with 2-deoxy-D-glucose as the substrate.

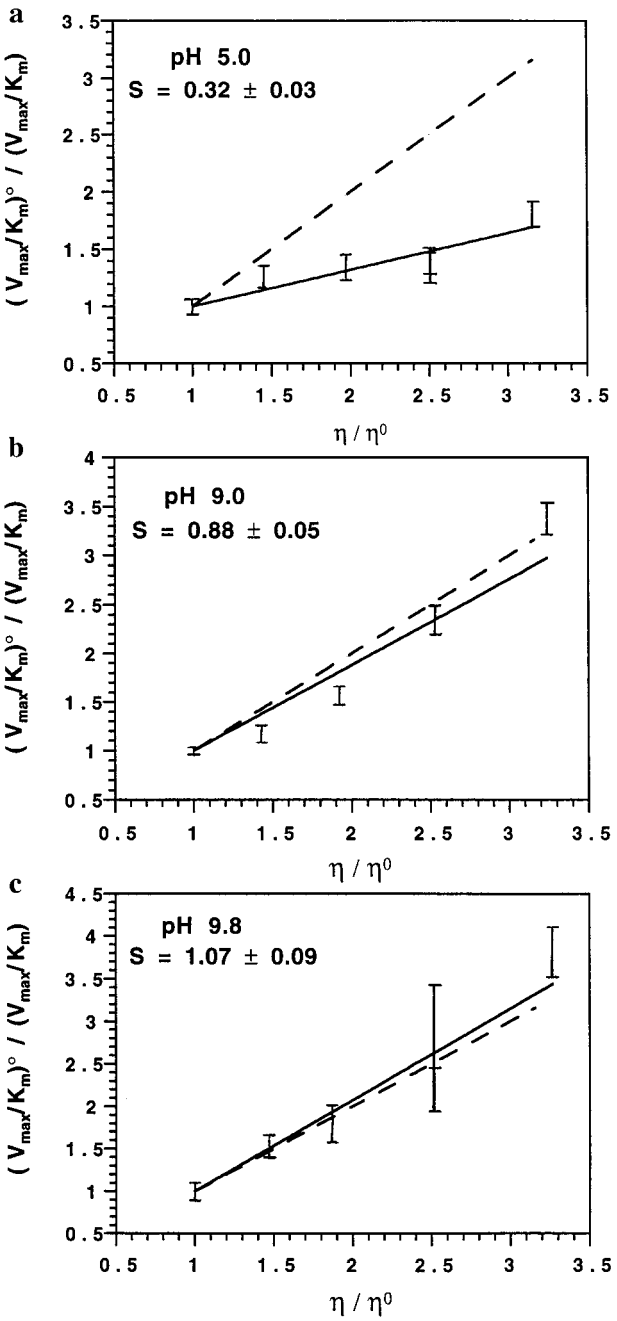

FIGURE 5: Effect of viscosity on $V_{max}/K_m(O_2)$ when ethylene glycol is used as the viscosogen at (a) pH 5.0, (b) 9.0, and (c) 9.8. The dashed line is the theoretical behavior for a 100% diffusion-controlled bimolecular reaction. The solid lines are obtained from fitting to eq 9.

The viscosity effects on $V_{max}/K_m(O_2)$ for pH 5.0, 9.0, and 9.8 are summarized in Figure 5, in comparison with the theoretical behavior for a fully diffusion-controlled bimolecular reaction (dashed lines). The data are fit to the following equation:

$$\frac{(V_{max}/K_m)^\circ}{(V_{max}/K_m)} = S(\eta_{rel} - 1) + 1 \qquad (9)$$

where $(V_{max}/K_m)^\circ$ is from the reference solution (without ethylene glycol), η_{rel} is the relative viscosity, and the slope S reflects the degree of viscosity dependence. At pH 5.0, $V_{max}/K_m(O_2)$ is 32% viscosity-dependent, and the dependence

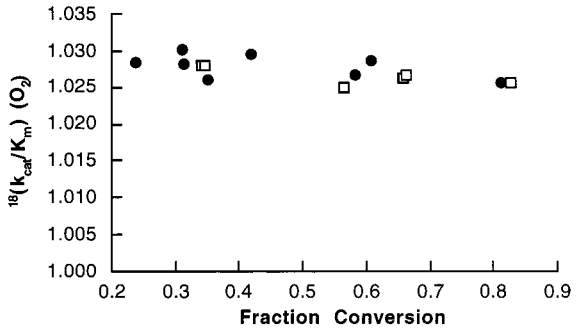

FIGURE 6: ^{18}O isotope effects. Data were acquired at pH 5.0 (●) and 9.0 (□). The average $^{18}(V_{max}/K_m)$ is 1.028 ± 0.2 at pH 5.0 and 1.027 ± 0.1 at pH 9.0.

increases to 88% at pH 9.0 and ca. 100% at pH 9.8. This observation supports the two-state model where both protonated and deprotonated forms of GO are active via different mechanisms: the oxygen binding step is rate-limiting and irreversible at high pH, while this oxygen association step must be reversible at low pH. According to eq 9, the $V_{max}/K_m(O_2)$ for protonated GO in D_2O [$\eta_{rel} = 1.25$, vs H_2O (*24*)] is expected to decrease from 1.6×10^6 (in H_2O) to 1.4×10^6 M^{-1} s^{-1}, and that for deprotonated GO is expected to decrease from 1.4×10^4 to 1.1×10^4 M^{-1} s^{-1}. Both of these calculated values are within experimental error of observed rates in D_2O (see Solvent Isotope Effects). We conclude that the rate decrease induced by D_2O can be fully ascribed to the change in solvent viscosity, ruling out any significant kinetic solvent isotope effects.

^{18}O Isotope Effects. The viscosity effect study brings about a result which is very curious and yet considerably mechanistically significant. Specifically, how do we explain the fact that the faster rate at low pH (1.6×10^6 M^{-1} s^{-1}) occurs in a less diffusion-controlled manner than the slower rate at high pH (1.4×10^4 M^{-1} s^{-1})? The measurement of heavy atom isotope effects has proven valuable in sorting out this dilemma. Using the methodology developed by Tian and Klinman (*25*), small ^{18}O isotope effects can be obtained reproducibly by isolating unreacted, natural abundance molecular oxygen from reaction mixtures, converting it quantitatively to carbon dioxide, and measuring the ratio of ^{16}O to ^{18}O in the carbon dioxide by isotope ratio mass spectrometry. The results obtained with GO are shown in Figure 6. The average values of $^{18}(V_{max}/K_m)$ are 1.027 ± 0.001 at pH 9.0 and 1.028 ± 0.002 at pH 5.0. The very sizable isotope effects indicate a change in bond order at dioxygen in the rate-limiting step. Quite unexpectedly, the magnitude of the $^{18}(V_{max}/K_m)$ does not change appreciably with pH, despite the large change in rate and degree of dependence on solvent viscosity. Previously calculated ^{18}O isotope effects for the stepwise reduction of dioxygen to hydrogen peroxide are summarized in Table 1 as a frame of reference. As expected, the magnitude of the ^{18}O effect reflects the bond order to oxygen, with electron transfer reducing the bond order (and increasing the isotope effect), while protonation at oxygen increases the bond order (and therefore decreases the ^{18}O effect). There are two circumstances that lead to isotope effects that are close to the experimental values (ca. 3%) seen with GO (Figure 6); these involve either a one-electron transfer to dioxygen (entry 1 in Table 1) or a two-electron, one-proton transfer to dioxygen (entry 3 in Table 1).

Table 1: ^{18}O Equilibrium Isotope Effects $^{18}(K)$ (*25*) and Reductive Half-Potentials (*26*) for the Stepwise Reduction of Dioxygen to Hydrogen Peroxide

Reaction	$^{18}(K)$	$\varepsilon°$ (mv) (pH 7)
$O_2 \overset{1e^-}{\rightleftharpoons} O_2^{\cdot-}$	1.0331	- 160
$O_2 \overset{1e^-,1H^+}{\rightleftharpoons} HO_2^{\cdot}$	1.0115	+ 120 (pH 1)
$O_2 \overset{2e^-,1H^+}{\rightleftharpoons} HO_2^-$	1.0340	+ 220
$O_2 \overset{2e^-,2H^+}{\rightleftharpoons} H_2O_2$	1.0089	+ 360

The high-pH form of GO provides a starting point for the integration of the rate, viscosity, and ^{18}O isotope effects measured in this study. Under these conditions, the reduction of dioxygen occurs in a close to diffusion-controlled step and exhibits an oxygen isotope effect close to that for full reduction of O_2 to superoxide anion. Although the redox potentials for superoxide anion [−160 mV vs SHE (*26*)] and enzyme-bound flavin [−240 mV vs SHE at pH 9.3 (*12*)] appear to be well-matched, we attribute the decreased rate at high pH relative to that at low pH to the absence of a counterion to stabilize the superoxide anion as it is formed. As noted above, the magnitude of the solvent isotope effect under these conditions is consistent with the diffusion-controlled nature of the reaction and fails to implicate any proton transfer in the course of the first electron transfer. The slow rate of the reaction compared to a typical diffusion rate constant (10^8−10^{10} M^{-1} s^{-1}) reflects the fact that this diffusional encounter occurs at an enzyme active site and, more importantly, is accompanied by an electron transfer; thus, the thermodynamic and reorganizational barriers that limit the electron transfer process contribute to the diffusion rate constant.

Interpretation of the low-pH data must integrate the fact that the reaction is less diffusion-controlled but exhibits the same ^{18}O isotope effect as seen at high pH. It is anticipated that once formed, the superoxide anion will combine with the flavin semiquinone to yield a flavin hydroperoxy intermediate. Structurally, this is very similar to HO_2^- and, hence, is expected to yield a value for $^{18}(K)$ of ∼3%. Thus, the most straightforward explanation for the observed data at low pH is the presence of two steps in $V_{max}/K_m(O_2)$, with both steps leading to intermediates having similar a bond order at dioxygen. We propose that the diffusional encounter, accompanied by one-electron transfer, has become less rate-limiting, revealing a second partially rate-limiting step in which the superoxide couples to the flavin semiquinone. Since $^{18}(K)$ is expected to be unchanged in going from superoxide anion to the flavin hydroperoxy intermediate, the experimental kinetic isotope effect may also exhibit this property.

A free energy profile contrasting the rate processes at high and low pH is given in Figure 7. As shown, the increased rate at low pH is due to an *increase* in the rate of the bimolecular one-electron transfer to dioxygen from the enzyme-bound reduced flavin. This is very different from the conventional observation of a change in diffusional control in enzyme reactions through the use of alternate substrates, which lead to a change in the reaction barrier height for the chemical step that follows binding (*23*). The rate increase with glucose oxidase occurs despite the fact that the flavin redox potential is less favorable for electron donation at low than at high pH [$\epsilon° = -65$ mV vs SHE at pH 5.3 (*27*)]. We conclude that the protonated His 516 exerts a *powerful* effect on the rate of production of the superoxide anion, leading to a *net* increase in catalytic efficiency of 2 orders of magnitude. If a correction is applied for the difference in redox potential for enzyme-bound FAD at high and low pH, *we estimate that the inherent rate acceleration may be as high as 5 orders of magnitude*. It is difficult to assess the effect of the protonation state of the histidine on the subsequent combination of the superoxide anion with the flavin semiquinone. As depicted in Figure 7, this process may actually be somewhat slowed as a result of a charge stabilization between the intermediate superoxide anion and protonated histidine. The mechanism that corresponds to Figure 7 is summarized in Scheme 2, where $k_1 \gg k_{1'}$.

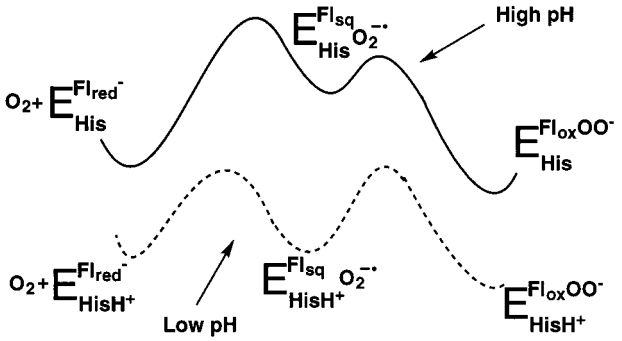

FIGURE 7: Comparative free energy profiles for the reaction of dioxygen with glucose oxidase at high and low pH, illustrating that the stabilization of $O_2^{-\bullet}$ anion by $HisH^+$ decreases the barrier for the first electron transfer from Fl_{red} to dioxygen, and that stabilization of the first intermediate could slow the second step.

Scheme 2: Proposed Mechanism for the Oxidative Half-Reaction in Glucose Oxidase

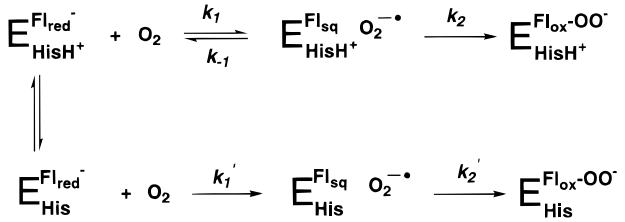

Simulation of the Oxidative Half-Reaction. The proposed model in Scheme 2 appears to suggest an accumulation of a semiquinone intermediate at low pH, which contrasts with previous failures to detect this intermediate at either low or high pH (*7*, *11*−*13*). However, the ability to detect this intermediate experimentally depends on the equilibrium constant of the first step; if the intermediate $Fl_{sq}{\cdot}O_2^{\bullet-}$ is high-energy and decomposes to Fl_{red} and dioxygen at a fast rate, no significant amount of semiquinone may accumulate.

A simulation for the reaction at low pH was carried out to examine this rationale and to estimate the boundaries for microscopic rate constants. The detailed mechanism and rate constants are described in Methods. The constraints on rate constants were obtained from viscosity studies; according to the proposed mechanism at low pH,

$$(V_{max}/K_m)^\circ = \frac{k_1 k_2}{k_{-1} + k_2} \quad (10)$$

$$(V_{max}/K_m) = \frac{(k_1/\eta_{rel})k_2}{(k_{-1}/\eta_{rel}) + k_2} \quad (11)$$

$$\frac{(V_{max}/K_m)^\circ}{(V_{max}/K_m)} = \frac{1}{k_{-1}/k_2 + 1}\eta_{rel} + \frac{k_{-1}}{k_{-1} + k_2} \quad (12)$$

$$\text{slope} = \frac{1}{k_{-1}/k_2 + 1} = 0.32;\ k_{-1}/k_2 = 2 \quad (13)$$

$$k_1 = (V_{max}/K_m)^\circ(k_{-1}/k_2 + 1) = 5.7 \times 10^6\ M^{-1}\ s^{-1} \quad (14)$$

The calculated values of k_1 and k_{-1}/k_2 (eqs 14 and 13, respectively) were fixed in each simulation. Noting that no flavin−hydroperoxy intermediate was detected (*7*, *11*−*13*), we assigned k_4 and k_3 (eqs 6 and 5, respectively) values so that $k_4 \gg k_3 \gg k_2$. Using the initial concentrations of 20 μM reduced GO and 640 μM O_2 [this concentration is used since in the most elaborate stopped flow UV−vis experiment described in the work by Stankovich et al (*12*), 1.27 mM O_2 was mixed with an equal volume of anaerobic reduced GO], the stopped flow traces were simulated with a wide range of k_{-1} values. Figure 8 illustrates some representative results. The simulations show that no significant amount of semiquinone intermediate accumulates if $k_{-1} > 5.7 \times 10^4\ s^{-1}$. When the fact that stopped flow experiments are limited by a dead time of ca. 1−2 ms is considered, the semiquinone intermediate can only be detectable if $k_{-1} \leq 5.7 \times 10^3\ s^{-1}$. The fact that all experiments failed to detect any intermediate implies that $5.7 \times 10^3\ s^{-1}$ is the lower limit for k_{-1}. A similar boundary for k_{-1} was obtained using other initial concentrations of O_2 in the simulations. With k_1 and the lower bound of k_{-1}, the redox potential $\epsilon_{O_2/O_2^{-\cdot}}$ can be calculated to be <0.11 V (vs SHE). Compared to the redox potential in aqueous solution, where $\epsilon_{O_2/O_2^{-\cdot}}$ is only -0.16 V [vs SHE (*26*)], the enzyme may provide up to 0.27 V of stabilization energy for the superoxide anion.

DISCUSSION

A series of kinetic probes have been applied in an attempt to elucidate the mechanism of dioxygen reduction in GO and to identify the strategy that the enzyme uses to facilitate effective catalysis. A two-state model, where protonated and deprotonated forms are both active and yet have 100-fold different reactivities, is presented and is based on the pH dependence of $V_{max}/K_m(O_2)$ (Figure 2) and the change of viscosity effects on $V_{max}/K_m(O_2)$ (Figure 5). At high pH, the close to 100% diffusion-controlled $V_{max}/K_m(O_2)$ (Figure 5) indicates that the bimolecular encounter of dioxygen with GO is rate-limiting in $V_{max}/K_m(O_2)$, and the magnitude of the ^{18}O isotope effect (ca. 3%, Figure 6) suggests that the

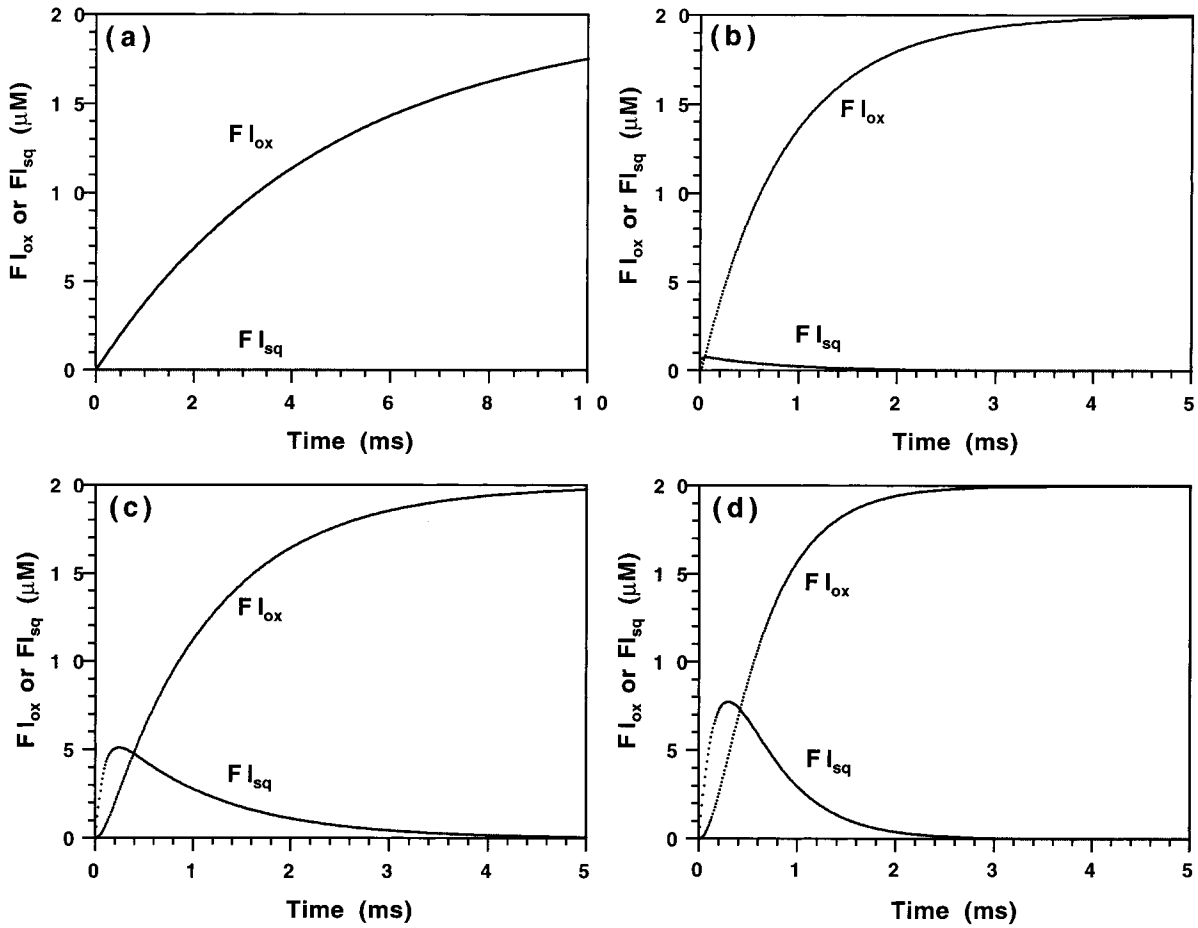

FIGURE 8: Simulation of the oxidative half-reaction at low pH. The dioxygen concentration is 640 μM, and the ratio of k_{-1} to k_2 is 2. See Methods for further details. The time course of Fl_{sq} is compared to the trace of Fl_{ox}. In all simulations (a−d), $k_1 = 5.7 \times 10^6\ M^{-1}\ s^{-1}$. In simulations b−d, $k_3 = 5.0 \times 10^5\ s^{-1}$ and $k_4 = 5.0 \times 10^6\ s^{-1}$. In simulation a, $k_{-1} = 5.7 \times 10^5\ s^{-1}$, $k_3 = 5.0 \times 10^6\ s^{-1}$, and $k_4 = 5.0 \times 10^7\ s^{-1}$. In simulation b, $k_{-1} = 5.7 \times 10^4\ s^{-1}$. In simulation c, $k_{-1} = 5.7 \times 10^3\ s^{-1}$. In simulation d, $k_{-1} = 5.7 \times 10^2\ s^{-1}$.

FIGURE 9: Segment of the sequence alignment of glucose oxidases, alcohol oxidases, and cholesterol oxidases. Protein sequences are from Entrez (Internet address http://www.ncbi.nlm.nih.gov/Entrez/); sequence IDs (in order from top to bottom) are 3023881, 1575046, 442927, 113652, 2104963, 231528, 466945, 1449378, and 443452. Sequence alignment was computed at GenomeNet CLUSTALW Server (Internet address http://www.clustalw.genome.ad.jp/), using BLOSUM scoring matrix, a gap open penalty of 10, and a gap extension penalty of 0.05.

association of dioxygen is accompanied by the first electron transfer, forming superoxide anion at the binding step. The proposal of rate-limiting superoxide formation at high pH is consistent with the absence of a solvent isotope effect (Figure 3) in the sense that no proton transfer step is included in $V_{max}/K_m(O_2)$. At low pH, the observation that the viscosity dependence decreases to only 32% (Figure 5) implies that $V_{max}/K_m(O_2)$ includes not only a diffusional bimolecular encounter but also some later step(s). The possibility that at low pH dioxygen binds to GO without electron transfer was considered and ruled out by the following considerations: (i) dioxygen is known to be hydrophobic in nature (*28*) and in the absence of a metal is expected to bind within a hydrophobic pocket; (ii) dioxygen binds to GO as superoxide anion in a diffusion-controlled manner at high pH, implying that no hydrophobic patch is available in the active site of GO under this condition; and (iii) there is no negatively charged residue in the GO active site [Brookhaven Protein Data Bank file name 1GAL (*8*)] which could undergo protonation at low pH to generate a hydrophobic binding pocket. We have, therefore, assumed that at low pH the binding of dioxygen is also coupled to electron transfer, forming superoxide at the initial step. The unchanged ^{18}O isotope effect at pH 5 (ca. 3%, Figure 6) suggests that the collapse of the superoxide and Fl_{sq} radical pair to form the flavin−hydroperoxy intermediate, which resembles HO_2^- [ca. 3% $^{18}(K)$, Table 1], is the first irreversible step. This interpretation excludes any proton transfer steps from $V_{max}/K_m(O_2)$, in agreement with the observation of no solvent isotope effect (Figure 3).

The pK_a of 7.9 from the $V_{max}/K_m(O_2)$ profile is assigned to an active site histidine, which in its protonated form stabilizes the high-energy intermediate species superoxide anion through electrostatic or hydrogen bond interaction. In the active site of GO from *A. niger*, there are two histidines: His 516 and His 559 [Brookhaven Protein Data Bank file name 1GAL (*8*)]. His 516 is 3.80 Å away from the negatively charged N-1 of Fl_{red} anion, while His 559 is hydrogen bonded to E 412. Both histidines could therefore have an elevated pK_a due to a favored interaction in their protonated forms. Sequence alignment of three glucose oxidases from *A. niger*, *Penicillium amagasakiense*, and *Talaromyces flavus* shows that both His 559 and His 516 are conserved (result not shown). Two closely related enzymes are alcohol oxidase (AO, EC 1.1.3.13) and cholesterol oxidase (CO, EC 1.1.3.6), which catalyze reactions very similar to that of GO, the only difference being the oxidation of different substrates during the reductive half-reactions. It is very likely that a common strategy has evolved for catalysis of the oxidative half-reactions for GO, AO, and CO. Sequence alignment of the above three GOs along with three AOs (*Candida boidinii*, *Pichia angusta*, and *Pichia pastoris*) and three COs (*Mycobacterium leprare*, *Mycobacterium tuberculosis*, and *Brevibacterium sterolicum*) is shown in Figure 9. His 516 is strictly conserved among all of the GO, AO, and COs that were examined. In contrast, His 559

Table 2: Redox Potentials $\epsilon^{\circ}_{Fl_{sq}/Fl_{red}}$ and Second-Order Rate Constants for Oxidation of Fl_{red} by Dioxygen

	pH	$\epsilon^{\circ}_{Fl_{sq}/Fl_{red}}$ (mV, vs SHE)	k (M^{-1} s^{-1})
solution	9.3	−242[a]	1.3×10^3 (*34*)
GO	9.3	−240 (*12*)	1.4×10^4
GO	5.3	−65 (*12*)	1.6×10^6

[a] Calculated from an $\epsilon^{\circ}_{Fl_{sq}/Fl_{red}}$ of −172 mV (vs SHE) in solution at pH 7.0 (*27*), a pK_a of 6.7 for neutral Fl_{red} (*20*), and a pK_a of 8.3 for neutral Fl_{sq} (*20*).

is aligned with Asn in AO and CO. Therefore, it is more likely that the universally conserved His 516 is responsible for the common part of the enzymatic reactions, i.e., the oxidation of Fl_{red} by dioxygen.

As the electrostatic stabilizing agent, the protonated His at the active site lowers the energy of the first intermediate, leading to an observed rate enhancement of 100-fold at low pH. The redox potential $\epsilon^{\circ}_{Fl_{sq}/Fl_{red}}$ in GO at pH 9.3 is −240 mV (Table 2), almost identical to the corresponding value for free flavin (Table 2). The limiting $V_{max}/K_m(O_2)$ at high pH is $(1.4 \pm 0.8) \times 10^4$ M^{-1} s^{-1}, only ca. 10-fold faster than the uncatalyzed reaction (Table 2), indicating that the oxidative half-reaction in GO at high pH is similar to the oxidation of free Fl_{red} and is mainly uncatalyzed. In the active site of GO, a long α-helix consisting of residues 561−581 is located next to the flavin cofactor, with its N-terminus (δ^+) pointing toward the flavin (Figure 1). The helix could contribute to the 10-fold rate enhancement in high-pH GO versus the free flavin reaction through electrostatic stabilization of superoxide by the helix dipole. Note that the redox potential $\epsilon^{\circ}_{Fl_{sq}/Fl_{red}}$ in GO at pH 5.3 is shifted to −65 mV (Table 2), despite the fact that the Fl_{red} is still an anion at pH 5.6 [according to ^{15}N NMR studies (*22*)]. The positive shift of ca. 180 mV of the redox potential $\epsilon^{\circ}_{Fl_{sq}/Fl_{red}}$ indicates that Fl_{red} is a worse reductant at low pH due to stabilization of Fl_{red} by protonated His 516. However, an increase of the dioxygen oxidizing power by stabilization of the superoxide anion (up to ca. 270 mV) more than compensates for the decrease in the Fl_{red} reducing power, and a *net* rate acceleration of 100-fold is achieved. The enzyme seems to have evolved in such a way that it balances electrostatic interactions to achieve optimal catalysis.

Stabilization of superoxide anion by a proximal protonated His is also seen in dioxygen binding proteins, e.g., studies that show enhanced dioxygen affinity toward cobalt-substituted leghemoglobin as His becomes protonated (*29*). Can any generalizations be made regarding the mechanism of dioxygen activation from the studies presented here? Prior to our investigation of glucose oxidase, the mechanism of reduction of dioxygen in systems that contain both an organic cofactor and transition metal had been examined; these systems are tyrosine hydroxylase [a pterin- and iron-containing enzyme (*30*)] and bovine serum amine oxidase [a topa quinone- and copper-containing enzyme (*14*)]. In both of the earlier examples, evidence was presented for a rate-limiting step involving electron transfer from the reduced cofactor to enzyme-bound dioxygen prior to any binding interaction with active site metal ion. For both tyrosine hydroxylase and bovine serum amine oxidase, redox potentials for the semiquinone/reduced cofactor pair are expected to be considerably less well matched to superoxide than is the case for the bound flavin in glucose oxidase [$\epsilon^{\circ} = 260$ mV vs SHE at pH 7 for free pterin (*31*) and $\epsilon^{\circ} > 100$ mV vs SHE at pH 7 for free topa quinone (*14*, *32*)]. Analogous to glucose oxidase, neither tyrosine hydroxylase nor bovine serum amine oxidase shows any evidence for a rate-limiting proton transfer to accompany the slow electron transfer step. In these two metalloenzymes, the active site metal ions may provide substantial charge stabilization to the superoxide anion as it is formed. Additionally, there is evidence that the reduced topa cofactor in bovine serum amine oxidase is neutral, forming a radical cation upon electron transfer to dioxygen. In this instance, the cofactor is also expected to lower the barrier for electron transfer to dioxygen by generating a stabilizing counterion for the resulting superoxide. The argument that energy modulation of superoxide anion intermediate is the key in the catalysis of dioxygen reduction is supported by the work of Wang and Thorpe, who observed strong suppression of dioxygen reactivity upon binding of hydrophobic ligands due to desolvation of the active site and consequent destabilization of the superoxide anion intermediate (*33*).

Although it is premature to formalize a set of rules for dioxygen activation in biological systems, we propose the following guidelines on the basis of our studies to date. (i) Formation of superoxide is likely to be the major rate-limiting step in peroxide formation, consistent with the fact that the first electron transfer to dioxygen is an uphill thermodynamic process, in contrast to the exergonic nature of subsequent electron and proton transfer steps for the formation of hydrogen peroxide (and water). In this manner, superoxide intermediates are not expected to accumulate under steady-state turnover conditions. (ii) Proton transfer does not occur in a concerted manner; i.e., there is no evidence for general acid catalysis in electron transfer to dioxygen. (iii) Electrostatic stabilization is likely to play the major role in adjusting the energy of the superoxide anion intermediate and the reaction barrier leading to this reactive intermediate.

ACKNOWLEDGMENT

We acknowledge Professor Frank M. Raushel (Texas A&M University, College Station, TX) for kindly providing the SGI version of KINSIM and Dr. Amnon Kohen for generously providing the enzyme.

REFERENCES

1. Wilson, R., and Turner, A. P. F. (1992) *Biosens. Bioelectron. 7*, 165−185.
2. Kriechbaum, M., Heilmann, H. J., Wientjes, F. J., Hahn, M., Jany, K. D., Gassen, H. G., Sharif, F., and Alaeddinoglu, G. (1989) *FEBS Lett. 255*, 63−66.
3. Frederick, K. R., Tung, J., Emerick, R. S., Masiarz, E. F., Chamberlain, S. H., Vasavada, A., Rosenberg, S., Chakraborty, S., Schopter, L. M., and Massey, V. (1990) *J. Biol. Chem. 265*, 3793−3802.
4. Kohen, A., Jonsson, T., and Klinman, J. P. (1997) *Biochemistry 36*, 2603−2611.
5. Kalisz, H. M., Hecht, H. J., Schomburg, D., and Schmid, R. D. (1991) *Biochim. Biophys. Acta 1080*, 138−142.
6. Kalisz, H. M., Hendle, J., and Schmid, R. D. (1997) *Appl. Microbiol. Biotechnol. 47*, 502−507.
7. Gibson, Q. H., Swoboda, B. E. P., and Massey, V. (1964) *J. Biol. Chem. 239*, 3927−3934.
8. Hecht, H. J., Kalisz, H. M., Hendle, J., Schmid, R. D., and Schomburg, D. (1993) *J. Mol. Biol. 229*, 153−172.

9. Weibel, M. K., and Bright, H. J. (1971) *J. Biol. Chem. 246*, 2734−2744.
10. Bright, H. J., and Gibson, Q. H. (1967) *J. Biol. Chem. 242*, 994−1003.
11. Bright, H. J., and Appleby, M. (1969) *J. Biol. Chem. 244*, 3625−3634.
12. Stankovich, M. T., Schopfer, L. M., and Massey, V. (1978) *J. Biol. Chem. 253*, 4971−4979.
13. Nakamura, S., and Ogura, Y. (1968) *J. Biochem. 63*, 308−316.
14. Su, Q., and Klinman, J. P. (1998) *Biochemistry 37*, 20513−20525.
15. Voet, J. G., Coe, J., Epstein, J., Matossian, V., and Shipley, T. (1981) *Biochemistry 20*, 7182−7185.
16. Voet, J. G., and Andersen, E. C. (1984) *Arch. Biochem. Biophys. 233*, 88−92.
17. Rogers, M. J., and Brand, K. G. (1971) *Biochemistry 10*, 4636−4641.
18. Glasoe, P. D., and Long, F. A. (1960) *J. Phys. Chem. 64*, 188−190.
19. Barshop, B. A., Wrenn, R. F., and Frieden, C. (1983) *Anal. Biochem. 130*, 134−145.
20. Muller, F. (1991) in *Chemistry and Biochemistry of Flavoenzymes* (Muller, F., Ed.) pp 1−72, CRC Press, Boca Raton, FL.
21. Eberlein, G., and Bruice, T. C. (1983) *J. Am. Chem. Soc. 105*, 6685−6797.
22. Sanner, C., Macheroux, P., Ruterjans, H., Muller, F., and Bacher, A. (1991) *Eur. J. Biochem. 196*, 663−672.
23. Brouwer, A. C., and Kirsch, J. F. (1982) *Biochemistry 21*, 1302−1307.
24. Weast, R. C., Astle, M. J., and Beyer, W. H. (1983−1984) *CRC Handbook of Chemistry*, CRC Press, Boca Raton, FL.
25. Tian, G., and Klinman, J. P. (1993) *J. Am. Chem. Soc 115*, 8891−8897.
26. Sawyer, D. T. (1991) *Oxygen Chemistry*, Oxford University Press, New York.
27. Stankovich, M. T. (1991) in *Chemistry and Biochemistry of Flavoenzymes* (Muller, F., Ed.) pp 401−425, CRC Press, Boca Raton, FL.
28. Sawyer, D. T., Chiericato, G., Jr., Angelis, C. T., Nanni, E. J., Jr., and Tsuchiya, T. (1982) *Anal. Chem. 54*, 1720−1724.
29. Ikeda-Saito, M., Hori, H., Inubushi, T., and Yonetani, T. (1981) *J. Biol. Chem. 256*, 10267−10271.
30. Francisco, W. A., Tian, G., Fitzpatrick, P. F., and Klinman, J. P. (1998) *J. Am. Chem. Soc. 120*, 4057−4062.
31. Eberlein, G., Bruice, T. C., Lazarus, R. A., Henrie, R., and Benkovic, S. J. (1984) *J. Am. Chem. Soc. 106*, 7916−7924.
32. Mure, M., and Klinman, J. P. (1993) *J. Am. Chem. Soc. 115*, 7117−7127.
33. Wang, R., and Thorpe, C. (1991) *Biochemistry 30*, 7895−7901.
34. Buice, T. C. (1983) *Isr. J. Chem. 24*, 54−61.
35. Su, Q., and Klinman, J. P. (1999) in *Enzymatic Mechanisms* (Frey, P. A., and Northrop, D. B., Eds.) pp 20−31, IOS Press, Amsterdam.
36. Covington, A. K., Paabo, M., Robinson, R. A., and Bates, R. G. (1968) *Anal. Chem. 40*, 700−706.
37. Schowen, B., and Schowen, R. L. (1982) *Methods Enzymol. 87*, 551−606.

BI990044O